7 Remote sensing of glaciers

Bruce H. Raup[1], Liss M. Andreassen[2], Tobias Bolch[3] and Suzanne Bevan[4]

[1] *NSIDC, University of Colorado, Boulder, USA*
[2] *Norwegian Water Resources and Energy Directorate, Oslo, Norway*
[3] *University of Zurich, Zurich, Switzerland*
[4] *Swansea University, UK*

Summary

Many elements of the cryosphere respond to changes in climate, but mountain glaciers are particularly good indicators of climate change, because they respond more quickly than most other ice bodies on Earth. Changes in glaciers are easily noticed by specialists and non-specialists alike, in ways that other climate indicators, such as ocean temperature or statistics of atmospheric circulation indices, are not. Remote sensing methods are capable of measuring many parameters of mountain glaciers and the changes they exhibit, leading to greater insight into processes affecting changes in glaciers and, hence, climate.

Field-based measurements are indispensable, as they yield high-precision data and give key insights into processes. However, due to expense and difficult logistics, such measurements are limited to a small number of sites. Remote sensing can cover large numbers of glaciers per image, and some long-term data collections (e.g., Landsat) are available for free. Algorithms and computational resources are now capable of producing maps of glacier boundaries at useful accuracy over large regions in a short time. New sensors will be coming online soon that will continue and extend this capability.

Mass balance is an important parameter indicating the health of a glacier. Mass balance can be estimated from satellite data by the "geodetic method" of measuring volume changes, where the change in volume is estimated by subtracting two digital terrain models of the glacier surface. A more recent approach to detect mass changes in land ice is through measurement of the gravitational field using the Gravity Recovery and Climate Experiment (GRACE) satellite system, which measures changes in mass below the orbit track.

Advances have been made recently in remote sensing of glaciers on a number of fronts, including more complete and more accurate glacier inventories, improved glacier mapping techniques, and new insights from gravimetric satellites. Through international cooperative efforts such as the Global Land Ice Measurements from Space (GLIMS) initiative and the Global Terrestrial Network for Glaciers (GTN-G), satellite remote sensing of glaciers has led to the ability to produce glacier outlines quickly over large regions, leading to the production

Remote Sensing of the Cryosphere, First Edition. Edited by M. Tedesco.

Companion Website: www.wiley.com/go/tedesco/cryosphere

of nearly complete global glacier inventories. These remote sensing products are being used to better understand climate, hydrological systems, and water resources, as our environment continues to change.

7.1 Introduction

Many elements of the cryosphere respond to changes in climate, but mountain glaciers are particularly good indicators of climate change because they respond more quickly than most other ice bodies on earth (Lemke *et al.*, 2007; Kääb *et al.*, 2007). Changes in glaciers are easily noticed by specialists and non-specialists alike in ways that other climate indicators, such as ocean temperature or statistics of atmospheric circulation indices, are not.

The most important parameter indicating the health of a glacier is its mass balance – the difference between accumulation, in the form of snow, avalanches and wind-blown snow, and ablation, which occurs principally through melt for land-terminating glaciers and melt plus iceberg calving for glaciers terminating in lakes or the ocean. The elevation at which accumulation and ablation occur in equal amounts over the course of a year is known as the equilibrium line altitude, or ELA.

End-of-season mass balance can be measured at a point on a glacier, and this quantity is generally positive (mass gain) in the accumulation area above the ELA, and negative (mass loss) in the ablation area below the ELA. Integrating such point measurements over the entire surface of the glacier yields the mass balance for the whole glacier for that year. The quantity is usually expressed as a water-equivalent change in thickness, in meters. Changes in volume or mass, measured with remote sensing methods, can be related directly to *in situ* measurements of mass balance.

There are long records of field-based measurements of mass balance (e.g., Zemp *et al.*, 2009), and these are valuable due to their detail and record length. However, field measurements on glaciers are laborious and expensive, and thus remote sensing techniques are necessary to extend our understanding to larger spatial scales and more glacier systems.

Glacier volume or mass, and their changes, can be investigated through remote sensing observations of glacier area or length, changes in elevation inferred from digital elevation models of the glacier surface estimated at two different times, or the end-of-summer snow line, which approximates the ELA (Braithwaite, 1984; Rabatel *et al.*, 2005). The connection between glacier geometry, as seen in 2-D imagery and mass balance, is complex, so some sort of modeling must be done to relate the two. Simple glacier flow models, together with long records of glacier length, have been used to estimate changes in regional climate (Oerlemans, 2005).

To estimate total glacier volume over large areas from satellite imagery, scaling relationships between glacier length or area and thickness or volume have been used (Bahr *et al.*, 1997; Raper and Braitwaite, 2005; Radić and Hock, 2010). However, scaling approaches have large uncertainty and are suitable for large samples of glaciers only; the method can estimate the average volume, for example,

for a system of glaciers, but not an individual one. The uncertainties of the scaling approaches can be reduced by taking into account empirical relationships between the glacier shear stress and the topography. Recent modeling advances, based on these parameters, allow the calculation of an approximate glacier bed topography and, hence, the glacier thickness and volume (Farinotti *et al.*, 2009; Paul and Linsbauer, 2012).

Glacier monitoring has been an internationally coordinated activity since 1894 (Haeberli, 1998), yet only recently are we beginning to have a nearly complete and accurate map of glaciers on Earth. Following decades of field-based measurements, many national programs are using remote sensing techniques to map glaciers in their respective countries (Paul *et al.*, 2002; Casassa *et al.*, 2002; Bajracharya and Shrestha, 2011; Lambrecht and Kuhn, 2007; Andreassen *et al.*, 2008; Bolch *et al.*, 2010a). International initiatives such as Global Land Ice Measurements from Space (GLIMS; Raup *et al.*, 2007) are bringing these results together into a single database (http://glims.org) and are driving more analysis in order to complete the data set. Remote sensing data are now used to measure many parameters of glaciers, including location, areal extent and changes in area, mass and volume changes, ice velocity, distribution of supraglacial features such as rock debris, ponds, and lakes, steepness, distribution of glacier area over elevation, and others. The following sections give a brief overview of how satellite data can be used to derive many of these measurements from space.

7.2 Fundamentals

Optical satellite imagers (instruments that produce imagery) are much like modern digital cameras, in that they sense and record the intensity of electromagnetic radiation (radiance) in several different parts of the spectrum (called bands or channels), which can be combined or analyzed in many different ways to derive information about the materials on the ground (see also Chapter 2). Materials have unique reflectance spectra which depend on their molecular make-up. Figure 7.1 shows high resolution spectra of several materials typically found in images of glacierized terrain.

For example, the local maximum in the green part of the visible spectrum for deciduous vegetation is due to the chlorophyll content of the leaves. The reflectance is higher still in the near-infrared part of the spectrum. By contrast, fresh snow has high reflectance across the visible parts of the spectrum, then drops to much lower values in the infrared.

The shape of the reflectance curve of a material is known as its spectral signature. Automatic methods for discriminating materials on the basis of their different spectral signatures, specifically adapted to the task of mapping glaciers, rely on differences in spectral signature. For clean glacier ice, automatic methods can be used to discriminate glaciers from surrounding materials. Many glaciers have rock and morainal debris covering their surfaces, making it nearly impossible to

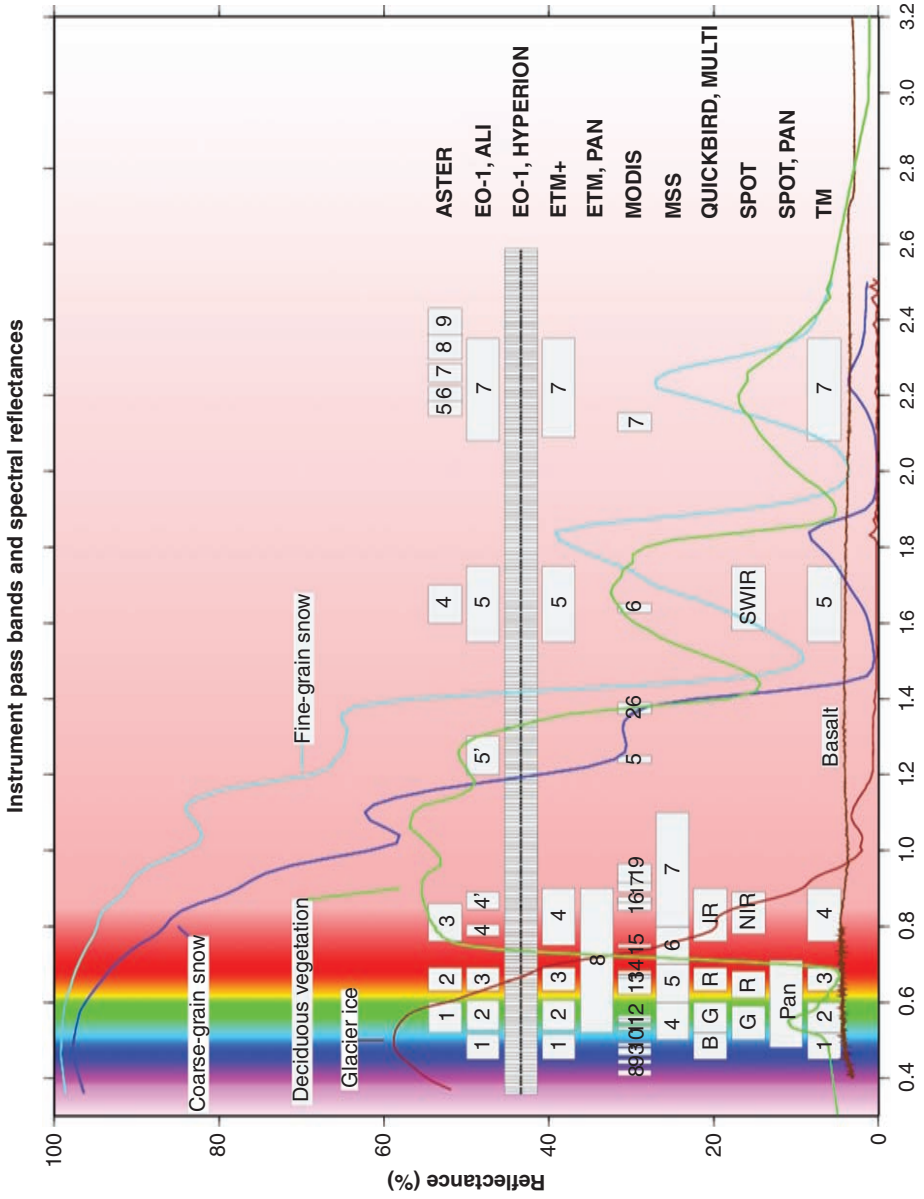

Figure 7.1 Reflectance spectra of several typical materials encountered in satellite imagery of glacierized terrain, and pass bands of several sensors in the visible and near-infrared (VNIR), and short-wave infrared (SWIR) parts of the spectrum.

discriminate between glacier debris cover and the rock, moraines, or forefield near the glacier. Other information must usually be brought to bear, which could be a digital terrain model or thermal information. Simple methods can be augmented with more sophisticated techniques, such as texture analysis or human interpretation, to compensate for the fact that debris-covered glacier ice is spectrally similar to surrounding materials.

Another challenge is determining locations of ice flow divides, where different parts of a contiguous ice mass flow in diverging directions. Ice flow divides generally mark a boundary between separate glaciers, but they are difficult to locate with precision and, typically, elevation data must be used in addition to satellite imagery to estimate ice flow directions.

Optical satellite sensors are characterized by several variables pertaining to their capabilities. Ground instantaneous field of view (GIFOV), which is closely related to spatial resolution, is the size of the area on the ground represented by one pixel in the image. Typically, the size of pixels and their spacing on the ground are essentially the same. Spectral resolution describes the number and spacing of pass bands along the electromagnetic spectrum. This determines the degree to which different materials on the ground can be discriminated.

The instruments discussed here are either multispectral instruments, which have 4–15 bands in the visible, near infrared, and thermal infrared, or hyperspectral instruments, which have hundreds of closely spaced bands. Additionally, some instruments record an integrated signal of radiance over the whole visible spectrum, and the resulting images are called panchromatic images. These are similar to black-and-white photographic images, which are also broadband in their response to light.

Another property is radiometric resolution, which is determined by the number of bits that are used to digitize the radiance signal produced by the light sensors. For example, an 8-bit system quantizes the radiance signal into 256 levels (i.e., 2^8, 0–255) or digital numbers (DN), whereas a 12-bit system produces 2^{12} (4096) levels. An instrument with low radiometric resolution can suffer from saturation of the DN values over bright targets (medium-bright to bright pixels set to the highest DN level), or only a few DN values being useful over dark targets. For example, variably bright snow in an 8-bit image may all be associated with the same DN value (255), while dark regions of the image that are in the shadow of a mountain may be represented by only a few DN values. Mapping the huge variations in brightness of a scene to only 255 levels would be similar to representing shoe sizes with only "small," "medium," and "large," rather than having a numeric scale with 30 levels. A 12-bit system, having 4096 levels, can represent a large range of brightness levels in a scene with high precision.

In addition to typical reflectance spectra, Figure 7.1 also shows the pass bands, or channels, for several optical satellite instruments that have been and are being used in glacier mapping. The primary workhorses for glacier mapping are multispectral imagers.

After their acquisition, raw images from a digital satellite sensor must be geometrically corrected so that the pixels represent a regular grid on the ground and are in a common map projection (e.g., Universal Transverse Mercator, UTM). This is

generally done by the data provider. An additional step, important for most glacier mapping efforts, is to orthorectify the imagery. In simple terms, orthorectification adjusts the locations of image pixels to correct for distortions caused by terrain. For example, the peak of a tall mountain on the left side of an image will appear closer to the left edge of the image than it should, due to parallax. Orthorectification corrects for this effect, and produces an image where it appears that the viewer is looking straight down (vertically) on all parts of the image (Schowengerdt, 2007).

7.3 Satellite instruments for glacier research

A variety of satellite data sources can be used for studying glaciers, from declassified Corona photographs (panchromatic images) through LANDSAT, Advanced Spaceborne Thermal Emission and Reflection Radiometer (ASTER), Satellite Pour l'Observation de la Terre (SPOT), to instruments recently or nearly online, such as the high spatial resolution Quickbird or Worldview satellites (Table 7.1).

The first spaceborne sensors to acquire imagery systematically were flying on the US Corona program strategic reconnaissance satellites, in operation between 1960 and 1972. The most useful characteristics of the Corona panchromatic images are their stereo capability and a spatial resolution of approximately 2–8 meters (Dashora *et al.*, 2007). Corona or other reconnaissance images such as Hexagon (see Table 7.1) have recently been used to map earlier extents of glaciers with high precision (Bhambri *et al.*, 2011; Narama *et al.*, 2010; Bolch *et al.*, 2010b), extending the observational record by a decade into the past.

A comprehensive and continuous survey of the Earth's surface began with the launch of the first LANDSAT satellite (originally called Earth Resources Technology Satellite, or ERTS-1) in 1972. The satellite carried the multispectral scanner (MSS), recording in four wavelength bands in the visible and near infrared spectrum with a GIFOV of about 80 m × 80 m. The first sensor to acquire data in the short wave infrared, which makes it suitable for automated glacier mapping, was the Thematic Mapper (TM) aboard the LANDSAT 4 satellite, launched in 1982.

The LANDSAT instruments, from the MSS through the TM instruments on LANDSAT 4 and 5, to the Enhanced Thematic Mapper Plus (ETM+) instrument on LANDSAT 7, have been particularly useful because they collectively cover a long time span and have a wide swath (185 km), allowing the coverage of large areas in one image. In addition, LANDSAT images are now available at no cost as orthorectified products (http://landsat.gsfc.nasa.gov/). The LANDSAT bands were selected to be able to measure radiance in parts of the spectrum with absorption features associated with a number of common natural materials, including bands in the visible and near-infrared (useful for distinguishing vegetation from rocks and from water), and bands in the thermal infrared (useful for measuring thermal inertia, temperature and temperature ranges). Other multispectral imagers, such as the French SPOT satellites, the Indian IRS (Indian Remote Sensing) satellites and the Japanese instrument ASTER on board the Terra satellite, have similar capabilities (e.g., Figure 7.2). Recent developments include ultra high resolution imagery

Table 7.1 Summary of characteristics for optical instruments suitable for mapping glaciers.

Platform	Instrument	Spectral bands	GIFOV (spatial resolution) [m]	Radiometric resolution [bits]	Swath [km]	Stereo	Time of operation
Corona	KH4, KH4-A, KH-4B	PAN	2–8	n/a	≈15 × 220	Yes	1960–1972
Hexagon	KH-9	PAN	6–10	n/a		Yes	1971–1986
LANDSAT 1-4	MSS	VNIR	≈79	8	183 × 172	No	1972–1993
Resurs-F1, Cosmos	KFA-1000	PAN, multi-spectral	5	n/a	75 × 75	Yes	1974–1999
Cosmos	KVR-1000	PAN	2	n/a	40 × 160	No	1981–2005
LANDSAT 4, 5	TM	VNIR, SWIR, TIR	30, 120	8	183 × 172	No	Since 1982
Cosmos	TK-350	PAN	10	n/a	200 × 300	No	Since 1984
SPOT 1	HRV	PAN, VNIR, SWIR	10, 20	8	60 × 60	No	1986–2002
Resurs-F2	MK-4	6, col, pan	6-12		144 × 144	Yes	1988–1995
SPOT2, 3	HRV	PAN, VNIR, SWIR	10, 20	8	60 × 60	Cross-track	Since 1990
IRS	LISS-III	VNIR, SWIR	5,6, 23, 70, 148	7	70 × 70, 140 × 140, 800 × 800	No	Since 1996
SPOT 4	HRVIR	PAN,VNIR,SWIR	10, 20, 1000	8	60 × 60, 2200 × 2200	Cross-track	Since 1998
LANDSAT 7	ETM+	PAN, VNIR, SWIR, TIR	15, 30, 60	8	183 × 172	No	Since 1999
Terra	ASTER	VNIR, SWIR, TIR	15, 30, 90	8	60 × 60	Along-track	Since 2000
Ikonos		PAN, VNIR	1, 4	11	11 × 14		Since 2000
Quickbird		PAN, VNIR	0.65, 2.7	11			Since 2001
SPOT 5	HRS/HRG	PAN, VNIR, SWIR	2,5, 5, 10, 1000	8	60 × 60, 1000 × 1000	Cross-track	Since 2002
IRS-P6	LISS-IV	VNIR, SWIR	5.8, 23.5, 56–70	7	24; 70, 140, 740	No	Since 2003
Cartosat-1 (IRS-P5)		PAN	2,5	12	30 × 30	Along-track	Since 2005
ALOS	PRISM	PAN	2.5	8	35 × 35, 70 × 70	Along-track	Since 2006
ALOS	AVNIR-2	VNIR	10	8	70 × 70	No	Since 2006
Worldview-2		PAN, VNIR	0.5, 1.8	11	16 × 16	Yes	Since 2009
LDCM (LANDSAT 8)	OLI, TIRS	PAN, VNIR, SWIR, TIR	15, 30, 100	12	185 × 180	No	Since 2013
Sentinel-2	MSI	PAN, VNIR, SWIR, TIR	10, 20, 60	12	290 × 290	No	2013 (sched.)

PAN = pan-chromatic. VNIR = visible and near infrared. SWIR = short-wave infrared.

Figure 7.2 (a) Example of an ASTER image, acquired 09-16-2010, of glaciers in the Chugach Range of southern Alaska. Bands 3N, 2, and 1 are displayed as red, green, and blue. (b) Oblique aerial photograph, taken in 1977, of Five Stripe Glacier, visible in the ASTER image at arrow. The snow line is clearly visible in (b) as the transition between bare glacier ice (gray) and snow (white), but the snow line in the ASTER image is almost above the highest elevation of Five Stripe Glacier.

with a resolution of one meter and below (e.g., Ikonos, Quickbird) and fast repeat cycles (e.g., Rapid-Eye).

The instruments described above are *passive*, in that they sense solar radiation scattered from the earth's surface (another class of instruments, "passive microwave sensors", measure microwave radiation emitted and reflected by surfaces). By contrast, radar instruments are *active* systems, where a beam is emitted from the sensor and the magnitude and phase of the backscattered energy is recorded. The United States SEASAT mission (1978) is regarded as the first satellite mission to carry a radar system, and was designed to measure surface properties and topography of the oceans (Evans *et al.*, 2005). Continuous radar missions that are useful for glaciological applications started only in the 1990s, with the European ERS-1, the Russian ALMAZ-1, and the Japanese, J-ERS-1 (Table 7.2).

Most satellite radar applications use synthetic aperture radar (SAR). The resolution of a radar image is inversely proportional to the size of the antenna (see also Chapter 9 for more on SAR and radar systems). The SAR technique synthesizes an antenna longer than is physically possible by using the constant velocity of the radar platform and knowledge of the changing geometry between the instrument and a given location on the ground. This technique increases the spatial resolution of radar systems by orders of magnitude.

Table 7.2 Important radar systems and their characteristics.

Platform	Instrument	Resolution (m)	Band	Pol.	Look angle (°)	Swath width (km)	Operation
SEASAT	SAR	25	L	HH	20	100	Jun–Sep 1978
ALMAZ-1	SAR	12–20	S	HH	25–60	40	1991
ERS-1	SAR	30	C	VV	23	100	1991–2000
J-ERS-1	SAR	18	L	HH	35	75	1992
Space Shuttle	SIR-C	15–25	L	Quad	20–55	30–100	1994
			C	Quad			
			X	VV			
ERS-2	SAR	30	C	VV	23	100	since 1995
Radarsat-1	SAR	10–100	C	HH	20–50	10–500	since 1995
SRTM	SAR	30	C	VV + HH	17–65	225	Feb. 2000
		30	X	VV	55	50	
ENVISAT	ASAR	30	C	Quad	15–45	100	2002–2012
		150				450	
ALOS	PALSAR	7–100	L	Quad	8–60	20–350	since 2006
Radarsat-2	SAR	3–100	C	Quad	10–60	20–500	since 2007
TerraSAR-X	SAR	3.3–17.6	X	Quad	20–60	10–100	since 2007
TanDEM-X	SAR	3.3–17.6	X	Quad	20–60	10–100	since 2010
Sentinel-x	SAR	5–40	C	Quad	20–45	80–400	2013 (sched.)

SAR = Synthetic Aperture Radar; ASAR = Advanced SAR; PALSAR = Phased-Array L-band SAR.

Other systems to measure surface elevation are laser and radar altimeters. Laser altimetry systems such as Geoscience Laser Altimetry System (GLAS), aboard the NASA Ice, Cloud, and land Elevation Satellite (ICESat), or radar altimetry systems such as the ENVISAT RA2 or CryoSat-2, transmit a pulse (laser light or radar beam) to the surface, and measure the time to receive the reflected response, thereby determining the elevation of the surface. ICESat GLAS was designed to study primarily the Greenland and Antarctic ice sheets, but has also been used to study mountain glacier elevation changes from space (Kääb, 2008; Moholdt *et al.*, 2010). The footprint of the transmitted spot for GLAS is approximately 70 m but, as the spacing of laser pulses on the ground is large compared to the size of most glaciers, this instrument can only be used to study a limited number of larger mountain glaciers or ice caps.

New satellites suited to studying mountain glaciers are planned to be launched in the near future. Particularly promising is the European Sentinel-2 satellite, scheduled to be launched in 2014, with a higher temporal and spatial resolution than the LANDSAT TM and ETM+ sensors. The LANDSAT Data Continuity Mission (LCDM) is valuable as well (Table 7.1).

7.4 Methods

7.4.1 Image classification for glacier mapping

Image classification is the process of assigning material classes (vegetation, rock, snow, water, etc.) to each pixel in an image. This first step is essential before creating a map of features (e.g., glaciers, lakes) in the imagery, although mapping features (e.g., glaciers) from a classified image (a map of materials) is not trivial, as many features involve a mixture of materials. For example, a glacier is dominantly ice, but it will often contain medial moraines or rock debris cover at the terminus, and the debris cover may even support vegetation. The "glacier" will therefore contain ice, rock, and vegetation classes in the classified image. Many different image classification and feature identification methods have been evaluated for glacier mapping, including manual digitization, supervised classification (maximum likelihood, minimum distance, spectral angle mapper, etc.), unsupervised classification, fuzzy classification techniques, and band arithmetic and threshold techniques (Sidjak and Wheate, 1999; Paul *et al.*, 2002; Albert, 2002; Racoviteanu *et al.*, 2009; Gjermundsen *et al.*, 2011).

Supervised classification begins with the operator selecting representative sets of pixels that are representative of identifiable materials in the image, such as vegetation, snow, glacier ice, and so on. The differences between the spectral signatures of these "training sets" (or end-members) are then used to assign the rest of the pixels in the image to one of those categories. Linear unmixing, a fuzzy classification technique, begins the same way but assigns fractional end-member content to each pixel. Unsupervised techniques such as ISODATA operate similarly, but

attempt to identify the end-members automatically by employing cluster detection algorithms. Details on image classification methods can be found in several books (e.g., Schowengerdt, 2007; Richards, 1986).

There is a trade-off between the time required to create glacier outlines from a method and the accuracy of the resulting outlines (Albert, 2002). Manual digitization, done by a glaciologist experienced in studying glaciers in remote sensing imagery, can achieve the highest accuracy in most types of terrain. Errors of interpretation can occur in some situations involving complicated patterns of debris cover on the glacier or seasonal snow attached to the glacier, but humans tend to do better in such situations than current computer algorithms. Mapping glaciers by hand, however, is the most time-consuming, and hence costly, of the available methods, and is therefore impractical for any but small regional studies.

Several studies (Albert, 2002; Paul *et al*., 2002; Racoviteanu *et al*., 2009) have concluded that the best trade-off between processing time and accuracy is obtained by band arithmetic techniques, such as computing band ratios or using normalized differences, such as the normalized difference snow index (NDSI; see also Chapter 3). In the band ratio technique, the ratio of bands in the near-infrared (NIR) or red parts of the spectrum and the short-wave infrared (SWIR) is computed, resulting in a "ratio image" that has high values over snow and ice, and low values over rock and vegetation. A threshold is applied to produce a binary raster mask indicating regions of snow/ice and non-snow/ice. Glacier outlines are then derived by converting the raster mask to a vector representation.

Both band ratios NIR/SWIR and red/SWIR have been shown to be well suited for glacier mapping, as they both take advantage of the large difference in spectral signature between snow and other materials in those spectral bands (Figure 7.1). Some studies have shown preference for Red/SWIR, as this discriminates better between ice and snow in shadow cast by adjacent terrain (Paul and Kääb, 2005). Andreassen *et al*. (2008) used the spectral characteristics of snow and ice in LANDSAT bands TM3 (Red) and TM5 (SWIR) for automatic classification of glaciers in Jotunheimen in southern Norway (Figure 7.3). The subset of the full scene used in their analysis contains neither clouds nor stark shadow, and there is no significant debris on the ice. The image is therefore well suited to the band ratio method.

The normalized difference snow index (NDSI; see also Chapter 3), another band arithmetic technique that is defined as (VIS-NIR)/(VIS + NIR), can be used similarly to map glacier outlines (e.g., Sidjak and Wheate, 1999; Racoviteanu *et al*., 2008b). For LANDSAT TM, for example, NDSI is obtained from the ratio (TM2-TM5)/(TM2 + TM5). It was developed to map snow (Hall *et al*., 1995; Salomonson and Appel, 2004; see Chapter 3), but since glacier ice is composed of densified snow, the spectral characteristics are similar (Figure 7.1). While the NDSI is useful for glacier mapping, the good performance and simplicity of the band ratio method for clean ice has resulted in the community predominantly using it to do classification (Racoviteanu *et al*., 2009). The band ratio method is easily automated but, as it relies on differences in spectral signatures of the materials in the image, it erroneously excludes parts of the glacier that are covered with rock debris. While newer techniques, discussed below, address these

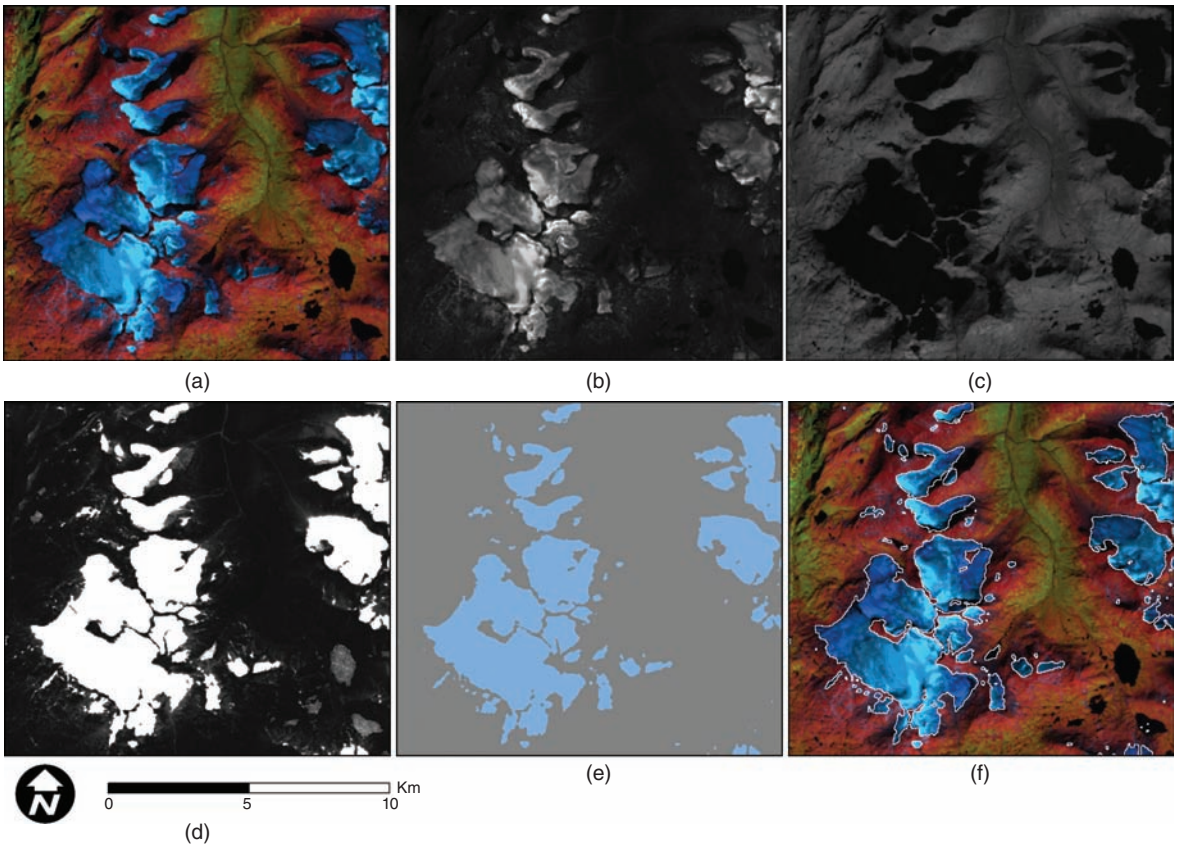

Figure 7.3 Automatic classification of snow and ice for a subset of glaciers in Jotunheimen, southern Norway, using a LANDSAT TM scene from 9 August 2003. (a) Red-green-blue (RGB) composite of TM bands 5, 4 and 3. (b) LANDSAT band TM3 (0.63–0.69 μm). (c) LANDSAT band TM5 (1.55–1.75 μm). (d) Ratio image of TM3/TM5. (e) Thresholded image of TM3/TM5 >2.0 and median filter (3 ∗ 3 kernel). (f) Same as (a), with outlines (in white) derived from raster to vector conversion of (e).

shortcomings, manual editing is generally needed to include debris-covered parts, to exclude seasonal snow and sometimes adjacent lakes, or to include parts of the glacier in heavy shadow.

7.4.2 Mapping debris-covered glaciers

More sophisticated methods than the ones presented above have been developed for automatically classifying debris-covered ice as part of the glacier. Some methods use thermal data, while others use topographic texture, curvature (geomorphometrics; Bishop *et al.*, 2001; Brenning, 2009), velocity, image differencing, or coherence images of SAR data (see next page) for detection of ice motion and to delineate the glacier boundary.

Finding the precise boundary of a glacier can be difficult, even for an experienced glaciologist in the field (Haeberli and Epifani, 1986), but it usually has characteristics that can be used to identify it, including distinctive morphology (such as a lateral concave-up trough or topographic drop at the terminus), or different thermal characteristics from surrounding rocks and tills. Semi-automated methods can also be used to detect glacier boundaries based solely on curvature of the DEM (Raup in Kieffer *et al*., 2000). This, and other similar approaches, show that even using only the morphology represented in the DEM can often lead to a good first estimate of the location of glacier boundaries.

Paul *et al*. (2004) developed a more automated algorithm which combines topographic information with multispectral imagery into a single algorithm. As a starting point, the algorithm uses a glacier ice region identified using the multispectral band ratio technique described above, and then expands this region, checking to ensure that pixels added to the region classified as "glacier" meet the following criteria:

a) the spectral signature is snow, ice, or rock;
b) the slope angle is low, below a specified threshold;
c) a concave-up area of curvature (a trough) has not been crossed.

Figure 7.4 shows the results of applying this algorithm to LANDSAT 5 (TM) imagery in the Bernese Alps, Switzerland. That study investigated two different DEMs as input – one based on ASTER, and one from the Swiss Federal Office of Topography. This general algorithm shows great promise, as most heavily debris-laden glaciers have similar morphological characteristics (e.g., low slope angles) to the ones investigated by Paul *et al*. (2004). However, the specifics must be modified, depending on the region. Stagnant ice that supports vegetation, varying regional glacier slope angles, icefalls, and heavy thermokarst activity (sub-debris melting, pond growth, and tunnel collapse) can all cause the algorithm to fail.

Another approach is to use the differing thermal properties of the supraglacial debris compared to surrounding rock. When the supraglacial debris is thin enough, the underlying ice cools the debris compared to surrounding rock and tills. For very thin debris, the intermittently exposed ice has a significant influence on the spectral signature of the pixels. Either of these two effects causes the debris-covered parts of the glacier to be distinguishable from the surrounding non-glacier material. Thicker debris violates these conditions, however, so this method appears to work well only for debris cover of less than about 0.5 m (Ranzi *et al*., 2004; Karimi *et al*., 2012). Thicker mantles of debris completely obscure the path of radiation between the ice and the sensor, as well as serving as an insulating layer which hides the cold surface of the ice. In addition, the spatial resolution of thermal data is invariably lower than visible and near-infrared imagery from the same platform, making it more difficult to apply such methods on smaller mountain glaciers. Further work is required to make thermally based methods capable of wide operational deployment.

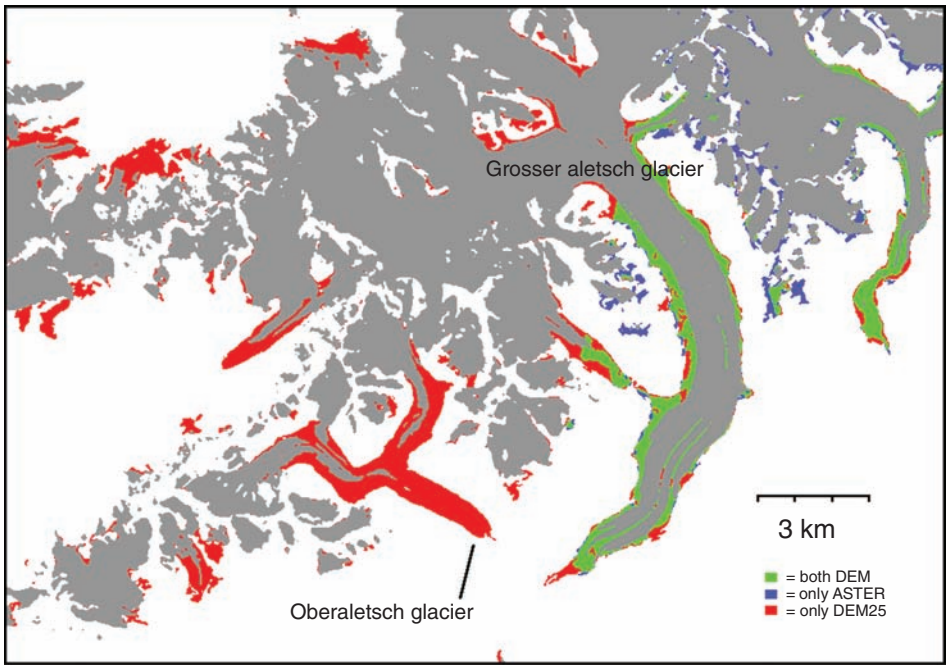

Figure 7.4 Results of applying a debris-covered glacier mapping algorithm to LANDSAT 5 imagery of the Bernese Alps, Switzerland, and two digital elevation models (adapted from Paul *et al.*, 2004).

7.4.3 Glacier mapping with SAR data

One main advantage of active radar systems is that they can operate in almost any weather as well as at night, because the beam and the backscattered radiation in the microwave region penetrate through clouds and do not depend on sunlight. In general, SAR data are capable of distinguishing snow and ice from surrounding areas, due to the different backscattering signal from different materials.

A limitation is that spaceborne satellite SAR systems are usually limited to one frequency of the emitted beam, which hampers the correct classification of glaciers (Rott, 1994). This is especially true if glaciers have variable surface roughness, for example due to crevasses, different snow and ice facies (snow, firn, glacier ice, refrozen melt water), and debris cover. The variable nature of the returned signal makes finding the glacier boundary difficult. Hence, SAR data has so far played only a minor role for glacier mapping.

An application where SAR performs better than optical methods in glacier studies is the discrimination of different snow facies. SAR data are often used to map temporal changes of snow and ice areas due to the temporal change of the surface's backscatter characteristics, best observable in the C band (4 to 8 GHz) and X band (8 to 12 GHz) (Nagler and Rott, 2000). The backscattering ratio of a summer and

winter image is used to discriminate between ice and snow in summer, while a winter image is best for obtaining the longer term ELA, because the SAR signal integrates over several meters depth in the snow pack and the boundary between ice and firn is therefore averaged over a few years (Floricioiu and Rott, 2001).

Recent efforts have focused on using SAR data for the detection of glaciers in areas with frequent cloud cover, and for debris-covered glaciers where the optical data are limited. One promising approach is the use of SAR coherence images (Atwood *et al.*, 2010), where areas with changing surfaces (e.g., due to glacier motion or down-wasting) decorrelate (the phase of the returned beam changes over time), in contrast to coherent stable areas. In addition, by taking advantage of the phase coherence of the transmitted radar beam, data from multiple passes can be analyzed for differences in the phase of the returned beam, which can be used for mapping topography, detecting subtle changes in the surface (including debris-covered areas), and mapping ice flow velocity. This technique is known as interferometric SAR, or InSAR (see Chapter 9 also for more InSAR applications).

Once glacier outlines are obtained by any method, basic glacier parameters, such as slope, aspect, elevation range, minimum, median, and maximum elevations, etc. can be obtained by examining DEM values within the outline or on the boundary (Paul *et al.*, 2009). Such parameters are generally stored as key parts of glacier inventories, such as the World Glacier Inventory and the GLIMS Glacier Database.

7.4.4 Assessing glacier changes

Time series of satellite imagery, or imagery combined with other data sources, can be used to detect and map changes in glacier extent, thickness, and surface characteristics.

When studying a series of images, the first step is to co-register them using ground control points (GCPs) or tie points. GCPs register the images to known locations on the ground, while tie points are features identifiable in both (or all) images, but may not be precisely located on the ground. This co-registration step is crucial, as many artifacts (false changes) can appear if there are offsets between the images. For change detection involving multi-temporal DEMs, proper co-registration is even more important, since improper co-registration leads to biases in the elevation differences everywhere in the domain, not just at the boundaries of different regions within the domain, as might be the case with classified imagery (Nuth and Kääb, 2011).

Changes in glacier area and length are easy to obtain directly from satellite observations, because they are directly related to changes in the observed two-dimensional (planimetric) information in the imagery. Changes in glacier volume or mass are more important scientifically (due to the connection to climate, and consequences such as sea level change or changes to hydrological resources), but they are more difficult to observe from satellite data.

7.4.5 Area and length changes

A simple yet effective way to detect change is the method of image differencing, where an earlier image is subtracted from a later one taken with identical or similar solar geometry (nearly the same time of day and day of year) (e.g., Sabins, 2007). The subtraction is usually done separately on each band, and results in a grid of numbers that are near zero in areas of no or little change, and which can be positive or negative for changed regions in the image. The grid is typically rescaled to positive numbers for display so that, for a single band, areas of no change appear gray, areas that have become more reflective (e.g., an area newly snow-covered) appear bright, and less reflective parts of the image (e.g., where snow or ice has been removed) look dark. Each difference band can be viewed on its own, or the rescaled difference bands can be displayed as red-green-blue, and the colors then yield information about changes in materials on the ground, since they indicate changes in spectral signature (e.g., by the appearance of vegetation on a moraine).

Mapping changes in glacier area based on repeat glacier extent mapping is straightforward in theory: create maps of glacier ice from two (or more) different images, and compare the computed areas. This can be done either from the raster map or from vector outlines that have been derived from a classified image. Another choice that the analyst must make is whether to compare maps of contiguous glacier ice as a whole, or to compare computed areas on a glacier-by-glacier basis. If the aim is to compute glacier area change for each separate glacier, great care must be taken to ensure that the ice divides (the boundaries between glaciers at their upper reaches) match exactly. If the ice divides do not match, then one can easily obtain the erroneous result that the glacier or glaciers on one side of a divide have grown, while those on the other side have shrunk, even if the total ice area did not change. This kind of investigation is therefore most safely performed over a whole system or mountain range (e.g., Racoviteanu *et al.*, 2008a).

Satellite imagery can also be used to derive length changes. High-resolution satellite imagery has been used to reconstruct glacier front variations over a period of four decades for the well-known Gangotri Glacier of northern India (Bhambri *et al.*, 2012). A study from Jostedalsbreen, Norway, showed that the high spatial variability measured from field data could be observed by LANDSAT (within one pixel, 30 m resolution) for glacier tongues not in cast shadow (Paul *et al.*, 2011).

As satellite imagery only goes back a few decades, it is common to assess glacier changes by comparing with other sources such as aerial photographs, topographic maps or inventory data (Casassa *et al.*, 2002). Glacier outlines derived from topographic maps are a valuable source, but they are usually mapped by non-glaciologists and might contain inaccuracies due to the existence of seasonal snow or misinterpretation of debris cover (Andreassen *et al.*, 2008; Bhambri and Bolch, 2009). Satellite imagery has also been used in several regions to map

glacier changes since the Little Ice Age maximum by mapping the glacier forefield, which is spectrally different from the terrain beyond the Little Ice Age maximum moraines (Paul and Kääb, 2005; Baumann *et al.*, 2009).

7.4.6 Volumetric glacier changes

DEMs can be used to measure volume changes of glaciers by subtracting pairs of DEMs. DEMs can be generated by different methods, such as space- and airborne optical stereo data, interferometric SAR (InSAR) data, space and airborne radar and laser altimetry, and topographic maps. There are three nearly global elevation products available today with high enough spatial resolution to study glacier changes:

1 The Shuttle Radar Topography Mission (SRTM) flown in February 2000.
2 ASTER Global DEM, version 2 (GDEM2) based upon stereo scenes acquired from 2000 to the present.
3 The ICESat mission from 2003 to 2009 using spaceborne laser altimetry, or Light Detection and Ranging (LiDAR).

These data sets all have different strengths and limitations. The SRTM DEM has relatively high resolution and covers the globe between 59°S and 60°N latitude, but it includes data voids in mountainous regions of high relief. Radar penetration of snow in the upper reaches of glaciers can lead to elevation biases there (Gardelle *et al.*, 2012). The ICESat elevation estimates are the most accurate (e.g., Nuth and Kääb, 2011), but the spatial coverage is much poorer, with 170 m spacing between points along-track and hundreds or thousands of meters between tracks, depending on latitude. Nevertheless, these data are valuable for obtaining region-wide information (Kääb *et al.*, 2012; Bolch *et al.*, 2013; Gardner *et al.*, 2013).

While the SRTM and standard ASTER DEMs have been proved to be useful as a baseline data set, more accurate DEMs are generally needed for precise volume change determination (e.g., Berthier *et al.*, 2010). Such DEMs can be created from individual image pairs from suitable optical stereo satellite instruments, such as ASTER, SPOT5, ALOS, and Cartosat-1 (e.g., Kääb *et al.*, 2012; Berthier *et al.*, 2007). LiDAR DEMs acquired using airborne systems are generally the most precise, but are limited to smaller areas. One of the largest ice bodies mapped nearly completely with LiDAR to date is Vatnajökull, the largest ice cap of Iceland (Johannesson *et al.*, 2012).

Elevation change of glaciers can be calculated by DEM differencing or repeat altimetry measurements (Figure 7.5). DEM differencing is a popular technique that has been used for decades to assess glacier changes (e.g., Finsterwalder, 1954; Abermann *et al.*, 2009). Changes in the volume of the glacier are converted to mass changes using estimates of density. This method is called the geodetic method

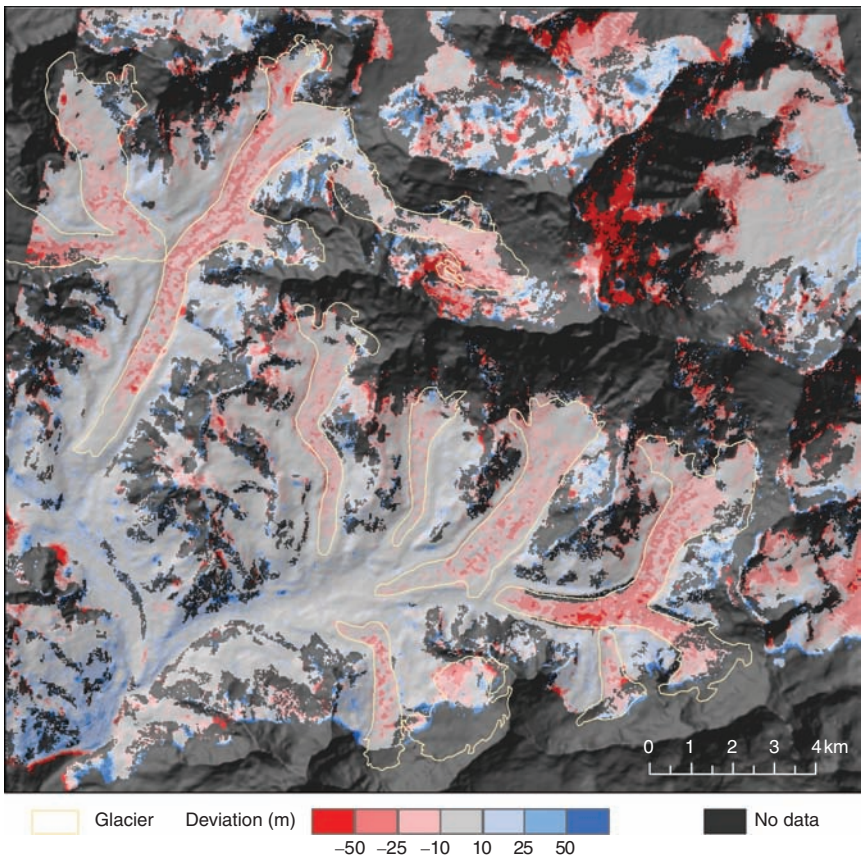

Figure 7.5 Glacier elevation changes measured by subtracting two DEMs in the Mt. Everest area of Nepal. DEMs are based on 1970 Corona and 2007 Cartosat data. Glacier outlines are plotted as light yellow lines (Bolch *et al.*, 2011).

of measuring mass changes and can be used to scale up to the whole glacier the traditional direct mass balance measurements based on field investigations, or to check their accuracy, or to assess changes in unmeasured areas or periods (e.g., Arendt *et al.*, 2002; Cogley , 2009; Fischer, 2010; Andreassen *et al.*, 2012).

7.4.7 Glacier velocity

There are two main techniques for deriving glacier surface flow velocities from remote sensing data:

1 tracking of features on the glacier's surface in sequential imagery, either optical or radar (feature tracking);
2 satellite radar interferometry (InSAR or D-InSAR) (Luckman *et al.*, 2007).

As in all methods for detecting change, feature tracking (Scambos *et al.*, 1992) requires that the input imagery should be accurately co-registered.

Feature tracking software, such as *IMCORR* or *Cosi-corr* (see Heid and Kääb (2012) for a comparison of algorithms), automatically finds matching features from both images and outputs a displacement vector for each location on a grid. For glaciers, these individual features could be ice pinnacles, crevasses, boulders, or a distinctive pattern of debris and ice, which can be identified on both images. Compared to field methods, where a day's work might produce a handful of velocity measurements for a glacier, feature tracking in satellite imagery is much more effective, yielding tens of thousands of vectors.

When feature tracking is applied to radar data, matching is generally done using the intensity images, which are images of the strength of the returned beam, either by tracking large-scale features that move with the ice and are visible in the imagery, or by tracking the small-scale pattern of light and dark in the intensity image that is due to phase coherence from one image to the next over stable surfaces. This latter technique is known as "speckle tracking," and it allows smaller patch sizes to be used compared to feature-tracking (Strozzi *et al*., 2002; Joughin, 2002). Studies that use feature tracking for velocity measurement include Kääb (2005), Bolch *et al*. (2008), Scherler *et al*. (2008), and Quincey *et al*. (2009).

Interferometric synthetic aperture radar (InSAR) is used for the observation of geometric displacements of the ground or glacier surface. Displacements on the order of centimeters or even millimeters can be measured, depending on the time difference between acquisitions. InSAR is based on the fact that the phase of the radar beam returned to the instrument from a spot on the ground does not change from overflight to overflight, provided the instrument is in the same position, unless the surface is changing. With two overflights, the phase part of the radar images can be subtracted to create an interferogram, which is a depiction of how the phase has changed from one overflight to the next. A single interferogram contains information about changes on the ground (deformation of the surface, or changed dielectric properties), as well as effects from differing satellite positions between overflights (orbital contributions) and topography. If the instrument is in slightly different positions for the two overflights, the effect on the interferogram can be modeled and removed.

To measure surface velocity with this technique, the effect of topography must be removed. This can be done using a DEM from an external source, such as SRTM or GDEM2, in which case only two satellite overflights are required (two-pass method). Alternatively, in the three-pass method, the first two images are used to generate a DEM. The time separation should be short between these two in order to minimize effects of surface deformation and, thus, decorrelation of the signal. The image of the third overflight is then used, together with the first or second image, to retrieve another interferogram. The second interferogram contains not only information about topography, but also the displacement, and by combining the two interferograms, the component of the ice velocity in the direction toward or away from the satellite sensor can be isolated.

The three-pass method is generally known as differential interferometric synthetic aperture radar, or D-InSAR. D-InSAR makes it possible to detect sub-meter changes in images that have a nominal ground resolution of several meters.

Problems with this technique for glacier velocity mapping include difficulty achieving the stability of the phase (phase coherence) necessary to make the method work, data availability, and layover (radar beam shadowing) in regions of high relief.

An example study using this technique is described in Yasuda and Furuya (2013), who studied short-term glacier velocity fluctuations in the Kunlun Shan range. More information about this technique can be found in Eldhuset *et al.* (2003) and Luckman *et al.* (2007).

7.5 Glaciers of the Greenland ice sheet

7.5.1 Surface elevation

The earliest satellite observations of surface elevation change over the Greenland ice sheet were based on radar altimeter data from the ERS-1 (1992 – 95) and ERS-2 (1995 – 2003) satellites (Johannessen *et al.*, 2005; Zwally *et al.*, 2005). The results indicated that the ice sheet was growing above the ELA and thinning at lower elevations, with an overall gain in volume. However, both studies indicated more rapid elevation increases at high elevations and less thinning over the margins than did results from repeat aircraft laser altimeter surveys within the same period (Krabill *et al.*, 2000). The differences at lower altitudes, where slopes are steeper, are probably due to the much larger footprint of the radar altimeter (≈20 km) compared with the 1 – 3 m airborne LiDAR footprint. At higher elevations, the difference may be due to changes in the radar penetration depth being superimposed on surface elevation changes (Thomas *et al.*, 2008).

Since 2002, the ICESat instrument GLAS, a laser altimeter, has been able to sample the faster-flowing outlet glaciers more precisely than the satellite radar altimeter systems, although the crossover points required to detect change are geographically sparse. Data from this instrument have shown that dynamic thinning is far more significant on the fast-flowing marine-terminating outlet glaciers than on the slower flowing parts of the ice sheet, and now reaches all latitudes in Greenland (Figure 7.6; Pritchard *et al.*, 2009). Chapter 8 contains more details on Accumulation and Surface Elevation techniques over Greenland.

7.5.2 Glacier extent

Observations of surface elevation change have focused attention on the frontal behavior, dynamics, and flow rates of the tidewater outlet glaciers in Greenland, where the greatest changes appeared to be concentrated.

The long archive of images from the LANDSAT series of satellites has proved to be particularly useful for monitoring the ice-front positions of these outlet glaciers all around the ice sheet. Manual identification of ice fronts in LANDSAT images, at multi-year intervals from 1972 to 2010, showed that marine-terminating glaciers

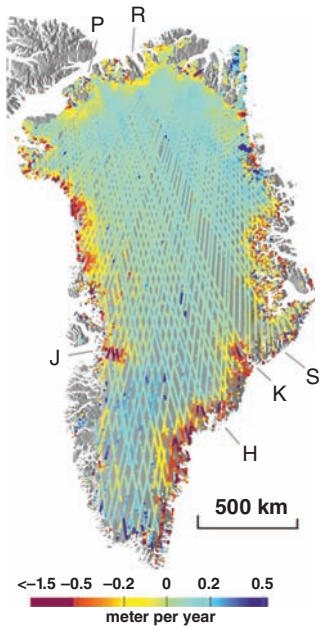

Figure 7.6 Rate of change of surface elevation for Greenland based on IceSAT GLAS data collected after 2002 (Pritchard *et al*., 2009). Major outlet glaciers are labeled: H – Helheim Glacier; K – Kangerdlussuaq Glacier; J – Jacobshavn Glacier; S – Sortebrae; P – Petermann Glacier, R – Ryder Glacier.

in the south-east and west were generally stable between 1972 and 1985, but began a gradual retreat in 1992, which accelerated between 2000 and 2010 (Howat and Eddy, 2011). A higher temporal resolution time series based on LANDSAT images identified a synchronous re-advance in 2006 in the southeast (Murray *et al*., 2010). The transition from stability to general retreat, which began in the early 1990s, was coincident with warming trends in land and sea surface temperatures (Howat and Eddy, 2011; Bevan *et al*., 2012).

Automating the identification of ice-fronts using edge-detection techniques on over 100 000 Moderate Resolution Imaging Spectroradiometer (MODIS) images allowed a ten-year daily time series of ice front positions to be produced for 32 east Greenland glaciers (Seale *et al*., 2011). In spite of the trade-off between revisit frequency (daily compared to 16 days in the case of LANDSAT) and spatial resolution (250 m, compared to 15 or 30 m for LANDSAT), a seasonal advance and retreat cycle of magnitude proportional to glacier width was identified. Ice fronts can be identified all year using SAR imagery, including during the polar night and when clouds obscure the ice fronts in optical imagery. This capability allows mosaics of the entire ice sheet to be generated for the same time of year at annual intervals, with the earliest coverage available in 1992. Moon and Joughin (2008) used SAR mosaics compiled for 1992, 2000, 2006 and 2007 to compare ice-front retreat rates between epochs and between land and tidewater terminating glaciers.

Occasionally, large individual calving events from Greenland outlet glaciers with floating tongues are observed in near real time in satellite imagery. For example, in August 2010, the Petermann Glacier in northern Greenland calved back by an estimated 28 km (Johannessen *et al*., 2011). The now multi-decadal archive of optical and SAR imagery allows these events to be placed in a longer term perspective.

7.5.3 Glacier dynamics

The retreat of outlet glacier ice fronts around the ice sheet often accompanies, or results in, an acceleration in ice flow via mechanisms which have yet to be fully understood (Joughin *et al.*, 2010). The application of feature-tracking and InSAR techniques has resulted in surface velocity measurements over large numbers of glaciers at multi-year intervals, in addition to high-resolution time series of measurements on individual glaciers.

Undoubtedly, the most dramatic stories for Greenland to be revealed, using remote sensing to measure ice velocities, concerned the rapid doubling or more of flow speeds by three major outlet glaciers. First, in the west, Jakobshavn Isbrae began speeding up in 1998 (Joughin *et al.*, 2004; Luckman and Murray, 2005) and then, in the southeast, Helheim began to accelerate around 2002, and Kangerlussuaq around 2004 (Howat *et al.*, 2005; Luckman *et al.*, 2006). The latter two have since decelerated, but both are still flowing faster than before (Howat *et al.*, 2007; Murray *et al.*, 2010).

In parallel with results for these individual glaciers, the mapping of surface velocities around the whole of Greenland showed a widespread acceleration south of 66°N between 1996 and 2000, which rapidly extended to 70°N by 2000 (Rignot and Kanagaratnam, 2006; Joughin *et al.*, 2010). Mirroring the pattern of ice-front retreat, feature tracking of early LANDSAT 5 images from 1985 has demonstrated that flow speeds were also stable around the ice sheet until temperatures began increasing in the mid-1990s (Bevan *et al.*, 2012). Moon *et al.* (2012) used data from a number of satellites to investigate changes in glacier speed for many of the ≈200 of Greenland's major outlet glaciers, and document complex patterns of velocity change that depend on glacier type (terminating in the ocean versus ice shelves versus land). These results indicate that the changes currently being experienced by Greenland's glaciers are more complex than previously thought. Underlying this complexity, however, appears to be an oceanic driver that is causing major changes in Greenland's outlet glaciers (Walsh *et al.*, 2012).

Comparing annual ice discharge flux for a glacier, based on remotely sensed flow speeds, with surface mass balance, allows an estimate of net mass balance for the catchment to be made. For example, in 1995/96, glaciers in the southeastern part of the ice sheet were shown to be flowing faster than was required to maintain balance (Rignot *et al.*, 2004). This flux-balance method also showed that, between 2000 and 2010, Jakobshavn Isbrae and Kangerdlugssuaq must have been losing mass, while Helheim was apparently gaining mass (Howat *et al.*, 2011).

Feature tracking and InSAR have also been used to investigate short-term variability in ice flow speeds. Examples include the surge of Sortebrae (Pritchard *et al.*, 2005), the mini-surge of Ryder Glacier and seasonal cycles of acceleration and deceleration on outlet glaciers (Luckman and Murray, 2005) and land-terminating sectors of the ice-sheet (Joughin *et al.*, 2008; Palmer *et al.*, 2011). Such short-term accelerations are thought to be driven by seasonal surface melt, percolating to the bed and increasing the basal water pressure, thereby enhancing basal lubrication

(Zwally *et al.*, 2002). Once an efficient subglacial drainage system is re-established, the flow speeds decrease again (e.g., Sundal *et al.*, 2011).

InSAR can be used not only to measure surface velocities, but also to identify parts of a glacier that are moving differently from other parts in a qualitative sense. InSAR analysis has been used, for example, to locate the boundaries of rock glaciers, which typically are spectrally indistinguishable from their surroundings, based on finding areas that are exhibiting creep. As another example, InSAR can be used to identify the location of grounding lines on glaciers with floating tongues. The grounding lines are indicated by the limit of tidal flexure revealed by differencing two velocity-only interferograms. This technique was used in northern Greenland to reveal the inland migration of grounding lines between 1992 and 1996, indicating glacier thinning with a dynamic origin (Rignot *et al.*, 2001).

7.6 Summary

Advances have been made recently in remote sensing of glaciers on a number of fronts, including more complete and accurate glacier inventories, improved glacier mapping techniques, and new insights from gravimetric satellites. Through international cooperative efforts such as the Global Land Ice Measurements from Space (GLIMS) initiative (Raup *et al.*, 2007) and the Global Terrestrial Network for Glaciers (GTN-G; Haeberli *et al.*, 2007), satellite remote sensing of glaciers has led to the ability to produce glacier outlines quickly over large regions, leading to the production of nearly complete global glacier inventories.

Another recent project, spurred by sea level modeling needs and deadlines of the Fifth Assessment Report of the Intergovernmental Panel on Climate Change (IPCC), has led to the production of a nearly globally complete set of glacier outlines, known as the Randolph Glacier Inventory (RGI). This data set lacks the thorough attributes and documentation of data sources of GLIMS data, but it has proved crucial to the IPCC work. For example, the glaciers and ice caps on and near Greenland have been completely mapped for the first time for the RGI (Figure 7.7; Rastner *et al.*, 2012). Both RGI and GLIMS outlines can be downloaded from the GLIMS website (http://glims.org). Glaciers from both GLIMS and the RGI in central Asia and the greater Himalayan region are being used for various ongoing projects (Figure 7.8). As discussed above, simple band ratio techniques can map glacier ice quickly, but debris cover remains a difficulty. More sophisticated techniques, such as texture analysis or the "fuzzy C-means" method (Schowengerdt, 2007), have yielded promising results for a wide range of glacier types (Racoviteanu *et al.*, 2009; Furfaro *et al.*, submitted).

Recent results from a completely different type of measurement, satellite gravimetry, have yielded direct estimates of mass changes in glacier ice. The Gravity Recovery and Climate Experiment (GRACE) system is a pair of satellites, orbiting in tandem, that use laser interferometry to measure the distance between

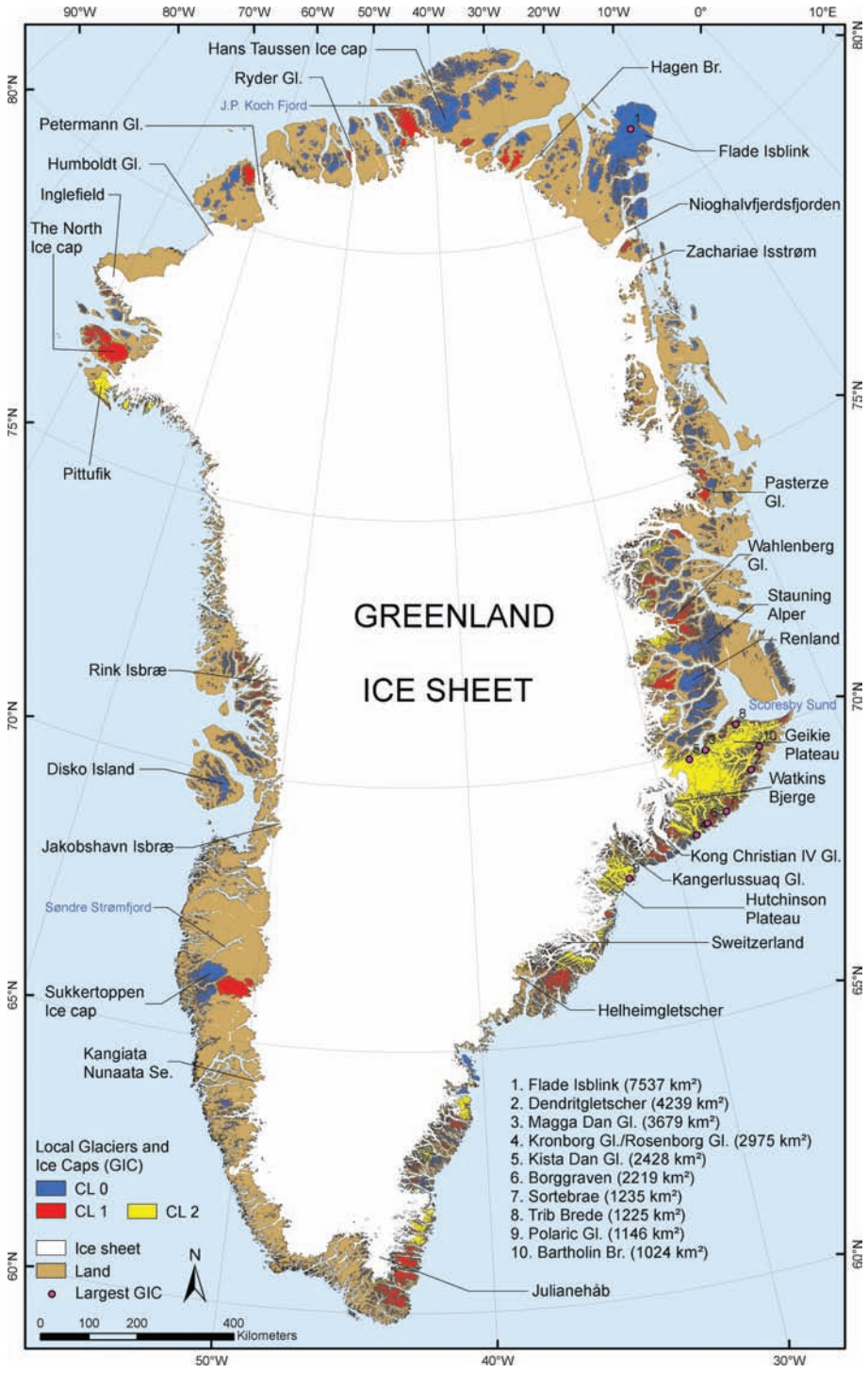

Figure 7.7 Map of glaciers and ice caps surrounding Greenland, obtained by automated application of the band ratio method to optical imagery, mostly LANDSAT (Rastner *et al.*, 2012).

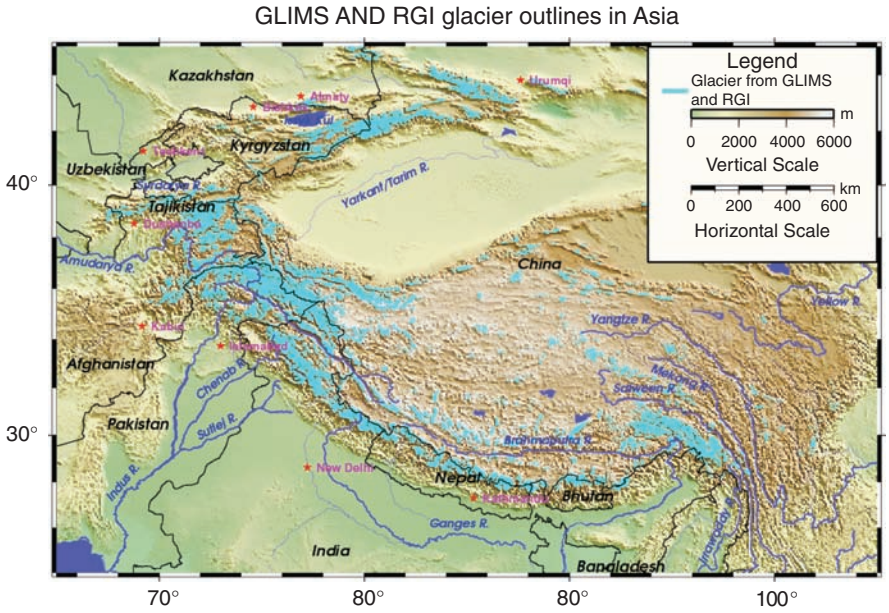

Figure 7.8 Glacier map for Central Asia, produced from GLIMS and RGI data sources using the GMT (Generic Mapping Tools) software.

the two satellites, producing information on changes in the gravitational field (Tapley *et al.*, 2004). One study applied GRACE data to measure glacier ice changes in all major glacierized regions on Earth (Jacob *et al.*, 2012). The spatial resolution of this technique is coarse (some 100 km) and the uncertainties are large compared to the signal in some regions (e.g., Himalaya), as the gravity signal depends on many other factors, including groundwater depletion and fluvial erosion. However, this method produces estimates of mass change that are independent of any other technique. It is probable that future systems will have better spatial resolution, and so will have better signal-to-noise performance (Silvestrin *et al.*, 2012).

In summary, remote sensing methods are capable of measuring many parameters of glaciers and glacier change, leading to greater insight into processes affecting changes in glaciers and hence climate. Field-based measurements are indispensable, as they yield high-precision data and give key insight into processes. However, due to expense and difficult logistics, such measurements are limited to a small number of sites. Remote sensing can cover large numbers of glaciers per image, and some long-term data collections (LANDSAT) are available for free. Algorithms and computational resources are now capable of producing maps of glacier boundaries at useful accuracy over large regions in a matter of days or hours. New sensors will be coming online soon that will continue and extend this capability. Gravitation-sensing satellites can directly measure changes in mass along their orbit tracks, though still at low resolution compared to individual glaciers.

References

Abermann, J., Lambrecht, A., Fischer, A. & Kuhn, M. (2009). Quantifying changes and trends in glacier area and volume in the Austrian Ötztal Alps (1969–1997–2006). *The Cryosphere* **3,** 205–215.

Albert, T.H. (2002). Evaluation of Remote Sensing Techniques for Ice-Area Classification Applied to the Tropical Quelccaya Ice Cap, Peru. *Polar Geography* **26**, 210–226.

Andreassen, L.M., Paul, F., Kääb, A. & Hausberg, J.E. (2008). LANDSAT-derived glacier inventory for Jotunheimen, Norway, and deduced glacier since the 1930s. *The Cryosphere* **2**, 131–145.

Andreassen, L.M., Kjøllmoen, B., Rasmussen, A., Melvold, K. & Nordli, Ø. (2012). Langfjordjøkelen, a rapidly shrinking glacier in northern Norway. *Journal of Glaciology*. Accepted.

Arendt, A.A., Echelmeyer, K.A., Harrison, W.D., Lingle, C.S. & Valentine, V.B. (2002). Rapid wastage of Alaska glaciers and their contribution to rising sea level. *Science* **297**(5580), 382– 386.

Atwood, D.K., Meyer, F. & Arendt, A.A. (2010). Using L-band SAR coherence to delineate glacier extent. *Canadian Journal of Remote Sensing* **36**(S1), S186.

Bahr, D.B., Meier, M.F. & Peckham, S.D. (1997). The Physical Basis of Glacier Volume-Area Scaling. *Journal of Geophysical Research* **102**, 20355–20362.

Bajracharya, S.R. & Shrestha, B.R. (Eds.) (2011). *The status of glaciers in the Hindu Kush-Himalayan Region*. ICIMOD, Kathmandu, Nepal.

Baumann, S., Winkler, S. & Andreassen, L.M. (2009). Mapping glaciers in Jotunheimen, South-Norway, during the "Little Ice Age" maximum. *The Cryosphere* **3**, 231–243.

Berthier, E., Arnaud, Y., Vincent, C. & Rémy, F. (2006). Biases of SRTM in high-mountain areas: Implications for the monitoring of glacier volume changes. *Geophysical Research Letters* **33**, L08502, doi:10.1029/2006GL025862.

Berthier, E., Arnaud, Y., Kumar, R., Ahmad, S., Wagnon, P. & Chevallier P. (2007). Remote Sensing Estimates of Glacier Mass Balances in the Himachal Pradesh (Western Himalaya, India). *Remote Sensing of Environment* **108,** 327–338.

Berthier, E., Schiefer, E., Clarke, G.K.C., Menounos, B. & Rèmy F. (2010). Contribution of Alaskan glaciers to sea-level rise derived from satellite imagery. *Nature Geoscience* **3**, 92–95, doi:10.1038/NGEO737.

Bevan, S.L., Luckman, A.J. & Murray, T. (2012). Glacier dynamics over the last quarter of a century at Helheim, Kangerdlugssuaq and 14 other major Greenland outlet Glaciers. *The Cryosphere Discussions* **6**, 1637–1672.

Bhambri, R. & Bolch, T. (2009). Glacier Mapping: A Review with special reference to the Indian Himalayas. *Progress in Physical Geography* **33**(5), 672–704.

Bhambri, R., Bolch, T., Chaujar, R.K. & Kulshreshtha S.C. (2011). Glacier changes in the Garhwal Himalaya, India, from 1968 to 2006 based on remote sensing. *Journal of Glaciology* **57**(203), 543–556.

Bhambri, R., Bolch, T. & Chaujar, R.K. (2012). Frontal recession of Gangotri Glacier, Garhwal Himalayas, from 1965–2006, measured through high resolution remote sensing data. *Current Science* **102**(3), 489–494.

Bishop, M., Bonk, R., Kamp, U. & Shroder, J. (2001). Terrain Analysis and Data Modeling for Alpine Glacier Mapping. *Polar Geography* **25**, 182–201.

Bolch, T., Buchroithner, M.F., Peters, J., Baessler, M. & Bajracharya, S. (2008). Identification of glacier motion and potentially dangerous glacial lakes in the Mt. Everest region/Nepal using spaceborne imagery. *Natural Hazards and Earth System Science* **8**, 1329–1340.

Bolch, T., Menounos, B. & Wheate, R. (2010a). LANDSAT-based Inventory of Glaciers in Western Canada, 1985–2005. *Remote Sensing of Environment* **114**, 127–137.

Bolch, T., Yao, T., Kang, S., Buchroithner, M.F., Scherer, D., Maussion, F., Huintjes, E. & Schneider, C. (2010b). A glacier inventory for the western Nyainqentanglha Range and Nam Co Basin, Tibet, and glacier changes 1976–2009. *The Cryosphere* **4**, 419–433.

Bolch, T., Pieczonka, T. & Benn, D.I. (2011). Multi-decadal mass loss of glaciers in the Everest area (Nepal Himalaya) derived from stereo imagery. *The Cryosphere* **5**, 349–358.

Bolch, T., Sandberg Sørensen, L., Simonssen, S.B., Mölg, N., Machguth, H., Rastner, P. & Paul, F. (2013). Mass loss of Greenland's glaciers and ice caps 2003–2008 revealed from ICESat laser altimetry data. *Geophysical Research Letters* **40**, doi: 10.1029/2012GL054710.

Braithwaite, R.J. (1984). Can the Mass Balance of a Glacier Be Estimated from Its Equilibrium-Line Altitude? *Journal of Glaciology* **30**(106), 364–368.

Brenning, A. (2009). Benchmarking classifiers to optimally integrate terrain analysis and multispectral remote sensing in automatic rock glacier detection. *Remote Sensing of Environment* **113**(1), 239–247.

Casassa, G., Smith, K., Rivera, A., Araos, J., Schnirch, M, & Schneider, C. (2002). Inventory of glaciers in Isla Riesco, Patagonia, Chile, based on aerial photography and satellite imagery. *Annals of Glaciology* **34**, 373–378.

Casey, K.A., Kääb, A. & Benn, D.I. (2012). Geochemical characterization of supraglacial debris via in situ and optical remote sensing methods: a case study in Khumbu Himalaya, Nepal. *The Cryosphere* **6**, 85–100.

Cogley, J.G. (2009). Geodetic and direct mass-balance measurements: comparison and joint analysis. *Annals of Glaciology* **50**(50), 96–100.

Dashora, A., Lohani, B. & Malik, J.N. (2007). A repository of earth resource information --- Corona satellite programme. *Current Science* **92**(7), 926–932.

Eldhuset, K., Andersen, P.H., Hauge, S., Isaksson, E. & Weydahl, D.J. (2003). ERS Tandem InSAR Processing for DEM Generation, Glacier Motion Estimation and Coherence Analysis on Svalbard. *International Journal of Remote Sensing* **24,** 1415–1437.

Evans, D.L., Alpers, W., Cazenave, A., Elachi, C., Farr, T., Glackin, D., Holt, B., Jones, L., Liu, W.T., McCandless, W., Menard, Y., Moore, R. & Njoku, E. (2005).

Seasat – A 25-year legacy of success. *Remote Sensing of Environment* **94**(3), 384–404. ISSN 0034–4257, 10.1016/j.rse.2004.09.011.

Farinotti, D., Huss, M., Bauder, A. & Funk, M. (2009). An estimate of the glacier ice volume in the Swiss Alps. *Global and Planetary Change* **68**(3), 225–231.

Finsterwalder, R. (1954). Photogrammetry and glacier research with special reference to glacier retreat in the eastern Alps. *Journal of Glaciology* **2**(15), 306–315.

Fischer, A. (2010). Glaciers and climate change: Interpretation of 50 years of direct mass balance of Hintereisferner. *Global and Planetary Change* **71**(1–2), 13–26.

Floricioiu, D. & Rott, H. (2001). Seasonal and short-term variability of multifrequency, polarimetric radar backscatter of Alpine terrain from SIR-C/X-SAR and AIRSAR data. *IEEE Transactions on Geoscience and Remote Sensing* **39**(12), 2634–2648.

Furfaro, R., Kargel, J. & Leonard, G. (submitted). Fuzzy C Mean Applications to and Validation of ASTER-Based Landcover Mapping of Root Glacier (Alaska). *The Cryosphere*.

Gardner, A.S., Moholdt, G., Cogley, J.G., Wouters, B., Arendt, A.A., Wahr, J., Berthier, E., Pfeffer, T.W., Kaser, G., Hock, R., Ligtenberg, S.R.M., Bolch, T., Sharp, M.J., Hagen, J.O., van den Broeke, M.R. & Paul, F. (2013). Narrowing the gap: A consensus estimate of glacier mass wastage. *Science*.

Gjermundsen, E., Mathieu, R., Kääb, A., Chinn, T., Fitzharris, B., & Hagen, J.O. (2011). Assessment of multispectral glacier mapping methods and derivation of glacier area changes, 1978–2002, in the central Southern Alps, New Zealand, from ASTER satellite data, field survey and existing inventory data. *Journal of Glaciology* **57**(204), 667–683.

Haeberli, W. (1998). Historical evolution and operational aspects of worldwide glacier monitoring. In: Haeberli, W., Hoelzle, M. & Suter, S. (eds). *Into the second century of worldwide glacier monitoring: prospects and strategies*, 35–51. UNESCO Studies and Reports in Hydrology.

Haeberli, W. & Epifani, F. (1986). Mapping the Distribution of Buried Glacier Ice – an Example from Lago Delle Locce, Monte Rosa, Italian Alps. *Annals of Glaciology* **8**, 78–81.

Haeberli, W., Hoelzle, M., Paul, F. & Zemp, M, (2007). Integrated monitoring of mountain Glaciers as key indicators of global climate change: the European Alps. *Annals of Glaciology* **46**, 150–160.

Hall, D.K., Riggs, G.A. & Salomonson, V.V. (1995). Development of Methods for Mapping Global Snow Cover Using Moderate Resolution Imaging Spectroradiometer Data. *Remote Sensing of Environment* **54**(2), 127–140.

Heid, T. & Kääb, A. (2012). Evaluation of existing image matching methods for deriving glacier surface displacements globally from optical satellite imagery. *Remote Sensing of Environment* **118**, 339–355.

Howat, I.M. & Eddy, A. (2011). Multi-decadal retreat of Greenland's marine-terminating glaciers. *Journal of Glaciology* **57**(203), 389–396.

Howat, I.M., Joughin, I., Tulaczyk, S. & Gogineni, S. (2005). Rapid retreat and acceleration of Helheim glacier, east Greenland. *Geophysical Research Letters* **32**, L22502.

Howat, I.M., Joughin, I. & Scambos, T.A. (2007). Rapid changes in ice discharge from Greenland outlet glaciers. *Science* **315**(5818), 1559–1561.

Howat, I.M., Ahn, Y., Joughin, I., van den Broeke, M.R., Lenaerts, J.T.M. & Smith, B. (2011). Mass balance of Greenland's three largest outlet glaciers, 2000–2010. *Geophysical Research Letters* **38**, L12501.

Jacob, T., Wahr, J., Pfeffer, T.W. & Swenson, S. (2012). Recent contributions of glaciers and ice caps to sea level rise. *Nature* **482**, 514–518.

Johannessen, O.M., Khvorostovsky, K., Miles, M.W. & Bobylev, L.P. (2005). Recent ice-sheet growth in the interior of Greenland. *Science* **310**, 1013–1016.

Johannessen, O.M., Babiker, M. & Miles, M.W. (2011). Petermann Glacier, North Greenland: massive calving in 2010 and the past half century. *The Cryosphere Discussions* **5**(1), 169–181.

Johannesson, T., Björnsson, H., Magnusson, E., Gudmundsson, S., Palsson, F., Sigurdsson, O., Thorsteinsson, T. & Berthier, E. (2012). Ice-volume changes, bias-estimation of mass-balance measurements and changes in subglacial lakes derived by LiDAR-mapping of the surface of Icelandic glaciers. *Annals of Glaciology* **54**(63).

Joughin, I. (2002). Ice-sheet Velocity Mapping: a Combined Interferometric and Speckle-tracking Approach. *Annals of Glaciology* **34**, 195–201.

Joughin, I., Abdalati, W. & Fahnestock, M. (2004). Large fluctuations in speed on Greenland's Jakobshavn Isbrae glacier. *Nature* **432**, 608–610.

Joughin, I., Howat, I., Alley, R.B., Ekstrom, G., Fahnestock, M., Moon, T., Nettles, M., Truffer, M., and Tsai, V.C. (2008). Ice-front variation and tidewater behavior on Helheim and Kangerdlugssuaq glaciers, Greenland. *Journal of Geophysical Research* **113**, F01004.

Joughin, I., Smith, B.E., Howat, I.M., Scambos, T. & Moon, T. (2010). Greenland flow variability from ice-sheet-wide velocity mapping. *Journal of Glaciology* **56**(197), 415–430.

Krabill, W., Abdalati, W., Frederick, E., Manizade, S., Martin, C., Sonntag, J., Swift, R., Thomas, R., Wright, W. & Yungel, J. (2000). Greenland ice sheet: High-elevation balance and peripheral thinning. *Science* **289**, 428–430.

Kääb, A. (2005). Combination of SRTM3 and Repeat ASTER Data for Deriving Alpine Glacier Flow Velocities in the Bhutan Himalaya. *Remote Sensing of Environment* **94**, 463–474.

Kääb, A., Chiarle, M., Raup, B. & Schneider, C. (2007). Climate Change Impacts on Mountain Glaciers and Permafrost. *Global and Planetary Change* **56**, vii–ix.

Kääb, A. (2008). Glacier Volume Changes Using ASTER Satellite Stereo and ICE-Sat GLAS Laser Altimetry. A Test Study on Edgeøya, Eastern Svalbard. *IEEE Transactions on Geoscience and Remote Sensing* **46**, 2823–2830.

Kääb, A. (2010). The role of remote sensing in worldwide glacier monitoring.In: Pellika, P. (ed). *Remote Sensing of Glaciers*, 285–296. CRC Press.

Kääb, A., Berthier E., Nuth, C., Gardelle, J. & Arnaud, Y. (2012). Contrasting patterns of early twenty-first-century glacier mass change in the Himalayas. *Nature* **488**(7412), 495–498.

Karimi, N., Farokhnia, A., Karimi, L., Eftekhari, M. & Ghalkhani, H. (2012). Combining optical and thermal remote sensing data for mapping debris-covered glaciers (Alamkouh Glaciers, Iran). *Cold Regions Science and Technology* **71**, 73–83.

Kieffer, H., Kargel, J.S., Barry, R. *et al.* (2000). New Eyes in the Sky Measure Glaciers and Ice Sheets. *Eos Transactions, American Geophysical Union* **81**(24), 265–271.

Lambrecht & Kuhn (2007). Glacier Changes in the Austrian Alps During the Last Three Decades, Derived from the New Austrian Glacier Inventory. *Annals of Glaciology* **46**, 177–184.

Lemke, P., Ren, J., Alley, R.B., Allison, I., Carrasco, J., Flato, G., Fujii, Y., Kaser, G., Mote, P., Thomas, R.H. & Zhang, T. (2007). Observations: Changes in Snow, Ice and Frozen Ground. In: Solomon, S., Qin, D., Manning, M., Chen, Z., Marquis, M., Averyt, K.B., Tignor, M. & Miller, H.L. (eds). *Climate Change 2007: The Physical Science Basis*. Contribution of Working Group I to the Fourth Assessment Report of the Intergovernmental Panel on Climate Change. Cambridge, UK and New York, NY, USA: Cambridge University Press.

Luckman, A., & Murray, T. (2005). Seasonal variations in velocity before retreat of Jakobshavn Isbrae, Greenland. *Geophysical Research Letters* **32**, L08501.

Luckman, A., Murray, T., de Lange, R., & Hanna, E. (2006). Rapid and synchronous ice-dynamic changes in east Greenland. *Geophysical Research Letters* **33**, L03503.

Luckman, A., Quincey, D. & Bevan, S. (2007). The potential of satellite radar interferometry and feature tracking for monitoring flow rates of Himalayan glaciers. *Remote Sensing of Environment* **111**(2–3), 171–181.

Moholdt, G., Nuth, C., Hagen, J.O. & Kohler, J. (2010). Recent elevation changes of Svalbard glaciers derived from ICESat laser altimetry. *Remote Sensing of Environment* **114**, 2756–2767.

Mool, P., Bajracharya S.R., Joshi S.P., Sakya K. & Baidya A. (2002). *Inventory of glaciers, glacial lakes and glacial lake outburst floods monitoring and early warning systems in the Hindu-Kush Himalayan region, Nepal*. International Center for Integrated Mountain Development (ICIMOD) tech. pub., 227 pp. Kathmandu, Nepal. ISBN 92 9115 345 1.

Moon, T. & Joughin, I. (2008). Changes in ice front position on Greenland's outlet glaciers from 1992 to 2007. *Journal of Geophysical Research* **113**, F02022.

Moon, T., Joughin I., Smith, B. & Howat, I. (2012). 21st-Century evolution of Greenland outlet glacier velocities. *Science* **336**(6081), 576–578.

Murray, T., Scharrer, K., James, T.D., Dye, S.R., Hanna, E., Booth, A.D., Selmes, N., Luckman, A., Hughes, A.L.C., Cook, S. & Huybrechts, P. (2010). Ocean regulation hypothesis for glacier dynamics in southeast Greenland and implications for ice sheet mass changes. *Journal of Geophysical Research* **115**, F03026.

Nagler, T. & Rott, H. (2000). Retrieval of wet snow by means of multitemporal SAR data. *IEEE Transactions on Geoscience and Remote Sensing* **38**(2), 754–765, doi:10.1109/36.842004

Narama, C., Kääb A., Duishonakunov, M. & Abdrakhmatov K. (2010). Spatial variability of recent glacier area changes in the Tien Shan Mountains, Central Asia,

using Corona (≈1970), LANDSAT (≈2000), and ALOS (≈2007) satellite data. *Global and Planetary Change* **71**(1–2), 42–54.

Nuth, C. & Kääb A. (2011). Co-registration and bias corrections of satellite elevation data sets for quantifying glacier thickness change. *The Cryosphere* **5**, 271–290.

Oerlemans, J. (2005). Extracting a Climate Signal from 169 Glacier Records. *Science* **308**, 675–677.

Palmer, S., Shepherd, A., Nienow, P. & Joughin, I. (2011). Seasonal speedup of the Greenland ice sheet linked to routing of surface water. *Earth and Planetary Science Letters* doi.org/10.1016/j.epsl.2010.12.037.

Paul, F. & Kääb, A. (2005). Perspectives on the production of a glacier inventory from multispectral satellite data in Arctic Canada: Cumberland Peninsula, Baffin Island. *Annals of Glaciology* **42**, 59–66.

Paul, F. & Linsbauer, A. (2012). Modeling of glacier bed topography from glacier outlines, central branch lines, and a DEM. *International Journal of Geographical Information Science* **1**, 1–18.

Paul, F., Kääb, A., Maisch, M., Kellenberger, T. & Haeberli, W. (2002). The new remote-sensing derived Swiss glacier inventory: I. *Methods. Annals of Glaciology* **34**, 355–361.

Paul, F., Huggel, C. & Kääb, A. (2004). Combining Satellite Multispectral Image Data and a Digital Elevation Model for Mapping Debris-covered Glaciers. *Remote Sensing of Environment* **89**, 510–518.

Paul, F., Barry, R.G., Cogley, J.G., Frey, H., Haeberli, W., Ohmura, A., Ommanney, C.S.L., Raup, B., Rivera, A., & Zemp, M. (2009). Recommendations for the Compilation of Glacier Inventory Data from Digital Sources. *Annals of Glaciology* **50**, 119–126.

Paul, F., Andreassen, L.M. & Winsvold, S.H. (2011). A new glacier inventory for the Jostedalsbreen region, Norway, from LANDSAT TM scenes of 2006 and changes since 1966. *Annals of Glaciology* **52**(59), 153–162.

Pritchard, H., Murray, T., Luckman, A., Strozzi, T. & Barr, S. (2005). Glacier surge dynamics of Sortebræ, east Greenland, from synthetic aperture radar feature tracking. *Journal of Geophysical Research* **110**, F03005.

Pritchard, H.D., Arthern, R.J., Vaughan, D.G. & Edwards, L.A. (2009). Extensive dynamic thinning on the margins of the Greenland and Antarctic ice sheets. *Nature* **461**(7266), 971–975.

Quincey, D.J., Luckman, A. & Benn, D. (2009). Quantification of Everest region glacier velocities between 1992 and 2002, using satellite radar interferometry and feature tracking. *Journal of Glaciology* **55**(192), 596–606.

Rabatel, A., Dedieu, J.P. & Vincent, C. (2005). Using remote-sensing data to determine equilibrium-line altitude and mass-balance time series: validation on three French glaciers, 1994–2002. *Journal of Glaciology* **51**(175), 539–546.

Racoviteanu, A.E., Arnaud, Y., Williams, M.W. & Ordonez, J. (2008a). Decadal Changes in Glacier Parameters in the Cordillera Blanca, Peru, Derived from Remote Sensing. *Journal of Glaciology* **54**, 499–510.

Racoviteanu, A., Williams, M.W. & Barry, R. (2008b). Optical remote sensing of glacier mass balance: a review with focus on the Himalaya. *Sensors*, Special issue: Remote sensing of the environment, 3355 – 3383.

Racoviteanu, A.E., Paul, F., Raup, B., Singh Khalsa, S.J. & Armstrong, R. (2009). Challenges and recommendations in mapping of glacier parameters from space: results of the 2008 Global Land and Ice Measurements from Space (GLIMS) workshop, Boulder, Colorado, USA. *Annals of Glaciology* **53**, 53 – 69.

Radić, V. & Hock, R. (2010). Regional and global volumes of glaciers derived from statistical upscaling of glacier inventory data. *Journal of Geophysical Research*, Earth Surface **115**, doi:10.1029/2009JF001373.

Ranzi, R., Grossi G., Iacovelli, L. & Taschner, S. (2004). *Use of multispectral ASTER images for mapping debris-covered glaciers within the GLIMS Project*. Proceedings of the International Geoscience and Remote Sensing Symposium 2004, 1144 – 1147.

Raper, S.C.B. & Braithwaite, R.J. (2005). The Potential for Sea Level Rise: New Estimates from Glacier and Ice Cap Area and Volume Distributions. *Geophysical Research Letters* **32**, doi: 10.1029/2004GL021981.

Raup, B., Kääb, A., Kargel, J.S., Bishop, M.P., Hamilton, G., Lee, E., Paul, F., Rau, F., Soltesz, D., Singh Khalsa, S.J., Beedle, M. & Helm, C. (2007). Remote Sensing and GIS Technology in the Global Land Ice Measurements from Space (GLIMS) Project. *Computers and Geosciences* **33**, 104 – 125.

Rastner, P., Bolch, T., Mölg, N., Machguth, H., Le Bris, R. & Paul, F. (2012). The first complete inventory of the local glaciers and ice caps on Greenland. *The Cryosphere* **6**, 1483 – 1495, www.the-cryosphere.net/6/1483/2012/, doi:10.5194/tc-6-1483-2012.

Richards, J.A. (1986). *Remote Sensing Digital Image Analysis*. Springer-Verlag Inc.

Rignot, E. & Kanagaratnam, P. (2006). Changes in the velocity structure of the Greenland ice sheet. *Science* **311**(5763), 986 – 990.

Rignot, E., Gogineni, S., Joughin, I. & Krabill, W. (2001). Contribution to the glaciology of northern Greenland from satellite radar interferometry. *Journal of Geophysical Research* **106**(D24), 34007 – 30019.

Rignot, E., Braaten, D., Gogineni, S.P., Krabill, W.B. & McConnell, J.R. (2004). Rapid ice discharge from southeast Greenland glaciers. *Geophysical Research Letters* **31**, L10401.

Rott, H. (1994). Thematic studies in Alpine areas by means of polarimetric SAR and optical imagery. *Advances in Space Research* **14**(3), 217 – 226.

Sabins, F.F., Jr. (2007). *Remote Sensing: Principles and Applications*, 3rd Edition. Long Grove, Illinois, USA. Waveland Press, Inc.

Salomonson, V.V. & Appel, I. (2004). Estimating fractional snow cover from MODIS using the normalized difference snow index. *Remote Sensing of Environment* **89**, 351 – 360.

Scambos, T.A., Dutkiewicz, M.J., Wilson, J.C. & Bindschadler, R.A. (1992). Application of Image Cross-Correlation to the Measurement of Glacier Velocity Using Satellite Image Data. *Remote Sensing of Environment* **42**, 177 – 186.

Scherler, D., Leprince, S. & Strecker, M.R. (2008). Glacier-surface velocities in alpine terrain from optical satellite imagery – accuracy improvement and quality assessment. *Remote Sensing of Environment* **112**(10), 3806–3819.

Schowengerdt, R.A. (2007). *Remote Sensing: Models and Methods for Image Processing*, 3rd Edition. San Diego, CA, Academic Press.

Seale, A., Christoffersen, P., Mugford, R.I. & O'Leary, M. (2011). Ocean forcing of the Greenland ice sheet: Calving fronts and patterns of retreat identified by automatic satellite monitoring of eastern outlet glaciers. *Journal of Geophysical Research* **116**, F03013.

Sidjak, R.W. & Wheate, R.D. (1999). Glacier Mapping of the Illecillewaet Icefield, British Columbia, Canada, Using LANDSAT TM and Digital Elevation Data. *International Journal of Remote Sensing* **20**, 273–284.

Silvestrin, P., Aguirre, M., Massotti, L., Leone, B., Cesare, S., Kern, M. & Haagmans, R. (2012). The Future of the Satellite Gravimetry After the GOCE Mission. In: Kenyon S. *et al*. (eds) *Geodesy for Planet Earth*, International Association of Geodesy Symposia **136**(2), 223–230, doi: 10.1007/978-3-642-20338-1_27.

Strozzi, T., Luckman, A., Murray, T., Wegmuller, U. & Werner, C.L. (2002). Glacier Motion Estimation Using SAR Offset-Tracking Procedures. *IEEE Transactions on Geoscience and Remote Sensing* **40**, 2384–2391.

Sundal, A.V., Shepherd, A., Nienow, P., Hanna, E., Palmer, S. & Huybrechts, P. (2011). Melt-induced speed-up of Greenland ice sheet offset by efficient subglacial drainage. *Nature* **469**(7331), 521–524.

Tapley, B.D., Bettadpur, S., Ries, J.C., Thompson, P.F. & Watkins, M.M. (2004). GRACE measurements of mass variability in the Earth system. *Science* **305**(5683), 503–505.

Thomas, R., Davis, C., Frederick, E., Krabill, W., Li, Y., Manizade, S. & Martin, C. (2008). A comparison of Greenland ice-sheet volume changes derived from altimetry measurements. *Journal of Glaciology* **54**(185), 203–212.

Walsh, K.M., Howat, I.M., Ahn, Y. & Enderlin, E.M. (2012). Changes in the marine-terminating glaciers of central east Greenland, 2000–2010. *The Cryosphere* **6**, 211–220.

Yasuda, T. & Furuya, M. (2013). Short-term glacier velocity changes at West Kunlun Shan, Northwest Tibet, detected by Synthetic Aperture Radar data. *Remote Sensing of Environment*, **128**, 87–106.

Zemp, M., Hoelzle, M. & Haeberli, W. (2009). Six decades of glacier mass-balance observations: a review of the worldwide monitoring network. *Annals of Glaciology* **50**, 101–111.

Zwally, H.J., Abdalati, W., Herring, T., Larson, K., Saba, J. & Steffen, K. (2002). Surface melt-induced acceleration of Greenland ice-sheet flow. *Science* **51**, 218–222.

Zwally, H.J., Giovinetto, M.B., Li, J., Cornejo, H.G., Beckley, M.A., Brenner, A.C., Sabba, J.L. & Li, D. (2005). Mass changes of the Greenland and Antarctic ice sheets and shelves and contributions to sea-level rise: 1992–2002. *Journal of Glaciology* **51**, 509–527.

Acronyms

ASTER	Advanced Spaceborne Thermal Emission and Reflection Radiometer
DN	Digital Numbers
ELA	Equilibrium Line Altitude
ERTS	1 Earth Resources Technology Satellite
ETM+	Enhanced Thematic Mapper Plus
GCP	ground control points
GIFOV	Ground instantaneous field of view
GLAS	Geoscience Laser Altimetry System
GLIMS	Global Land Ice Measurements from Space
GRACE	The Gravity Recovery and Climate Experiment
GTN-G	Global Terrestrial Network for Glaciers
ICESat	Ice, Cloud, and land Elevation Satellite
IPCC	Intergovernmental Panel on Climate Change
IRS	Indian Remote Sensing
LDCM LANDSAT	Data Continuity Mission
LIDAR	Light Detection and Ranging
MSS	Multispectral scanner
NDSI	normalized difference snow index
NIR	Near Infrared
RGI	Randolph Glacier Inventory
SPOT	Satellite Pour l'Observation de la Terre
SRTM	Shuttle Radar Topography Mission
SWIR	short-wave infrared
TM	Thematic Mapper
UTM	Universal Transverse Mercator

Websites cited

http://glims.org
http://landsat.gsfc.nasa.gov/